Functional heart recovery in an adult mammal, the spiny mouse

Yanfei Qi [a], Osama Dasa [b], Malcolm Maden [c], Ravneet Vohra [d], Abhinandan Batra [d], Glenn Walter [d], Joshua F. Yarrow [e], Juan M. Aranda Jr [a], Mohan K. Raizada [d], Carl J. Pepine [a],*

[a] Division of Cardiovascular Medicine, Department of Medicine, College of Medicine, University of Florida, Gainesville, FL, USA
[b] Department of Internal Medicine, University of Florida, Gainesville, FL, USA
[c] UF Genetics Institute and Department of Biology, University of Florida, Gainesville, FL, USA
[d] Department of Physiology and Functional Genomics, College of Medicine, University of Florida, Gainesville, FL, USA
[e] Malcom Randall VA Medical Center, Gainesville, FL, USA

ARTICLE INFO

ABSTRACT

Background: Ischemic heart disease and the resulting heart failure continue to carry high morbidity and mortality, and a breakthrough in our understanding of this disorder is needed. The adult spiny mouse (*Acomys cahirinus*) has evolved the remarkable capacity to regenerate full-thickness skin tissue, including microvasculature and cartilage, without fibrosis or scarring. We hypothesized that lack of scarring and resulting functional regeneration also applies to the adult *Acomys* heart.
Methods and results: We compared responses of the *Acomys* heart to CD1 outbred *Mus* heart following acute left anterior descending coronary artery ligation to induce myocardial infarction. Both *Acomys* and *Mus* hearts showed decreased ejection fraction (EF) after ligation. However, *Acomys* hearts showed significant EF recovery to pre-ligation values over four weeks. Histological analysis showed comparable infarct area 24-h after ligation with a similar collateral flow in both species' hearts, but subsequently, *Acomys* displayed reduced infarct size, regenerated microvasculature, and increased cell proliferative activity in the infarcted area.
Conclusions: These observations suggest that adult *Acomys* displays remarkable cardiac recovery properties after acute coronary artery occlusion and may be a useful model to understand functional recovery better.
Translational perspective: Adult *Acomys* provides a novel mammalian model to further investigate the cardioprotective and regenerative signaling mechanisms in adult mammals. This opens the door to breakthrough treatment strategies for the injured myocardium and help millions of patients with heart failure secondary to tissue injury with irreversible damage.

© 2021 Elsevier B.V. All rights reserved.

1. Introduction

Ischemic heart disease, particularly myocardial infarction (MI), continues as a major contributor to death, disability, and health resource consumption [1]. Despite advances in management that have markedly improved survival, subsequent cardiac remodeling and heart failure remain critical issues. A central problem in the ischemic-damaged adult mammalian heart is that necrotic myocardial tissue is replaced by non-contractile scar tissue, and spared tissue undergoes considerable remodeling in an attempt to recover ventricular contractile function. Thus, reducing cardiac damage and improving recovery following acute ischemic injury continue to be important targets for management.

In contrast, several non-mammalian vertebrate species such as Urodele amphibians and zebrafish possess a remarkable capacity for cardiac repair and regeneration after apical resection, cryoinjury, or genetic ablation [2] through dedifferentiation and proliferation of cardiomyocytes to replenish damaged myocardium [3,4]. This is also the basis of the regenerative ability of the 1-day-old mouse heart [5]. Regeneration of the mammalian heart has been thought to partially rely on endogenous cardiac stem cells' reactivation, followed by recruitment to the site of injury [6,7]. However, some have suggested that cardiomyocytes can also re-enter the cell cycle [8] through activation of the neuregulin1/ErbB4 signaling pathway [9]. These studies have thus driven a therapeutic approach to cardiac repair in the adult mammal that reawakens proliferative activity in quiescent cardiomyocytes to induce cardiac regeneration.

Strikingly, we and others have observed that the adult spiny mouse (*Acomys cahirinus*) can regenerate many tissues in response to full-thickness skin, skeletal muscle, ear punches, or kidney damage [10–15]. Consistently across these tissues, lack of fibrosis and collagen deposition in the wound contributes to the regeneration of microvessels, smooth muscle, skeletal muscle, adipose tissue, sebaceous glands, hair follicles, and even ear cartilage without scarring. This significant lack of scarring in *Acomys* skin prompted us to hypothesize that

the same property might be apparent in this adult mammal's heart, which would be very novel. Accordingly, we investigated the functional and cellular responses of the heart following ischemia/infarction-induced myocardial damage. We specifically sought to determine whether *Acomys* would show a reduced fibrotic reaction to ischemic injury and perhaps even improved functional capacity compared with reference CD1 *Mus* mice adults.

2. Methods

2.1. Animals and ethics statements

All animal procedures were approved by the Institutional Animal Care and Use Committee at the University of Florida (UF) and complied with the National Institutes of Health and USDA guidelines. Animals were maintained under a 12/12 h light/dark cycle at 25° ± 1 °C, with unrestricted access to food and water. *Acomys cahirinus* were produced from our colony housed at UF, and the CD1 *Mus* were purchased from Charles River. Male mice 3–6 months of age were used to avoid differential responses due to changing hormone levels. CD1 mice were used as a reference group as these are the most outbred strain available for comparison with another species and have been used as references in our previous studies of *Acomys* tissue regeneration [10,11].

2.2. Myocardial infarction

The mice were divided into four experimental groups: CD1-sham, CD1-MI, *Acomys*-sham, and *Acomys*-MI. Group sizes varied, initially *n* = 12 and in some repeated groups, *n* = 4. Surgical procedures were previously described with a few modifications [16]. Briefly, mice were anesthetized with 1.5–2% isoflurane (in 100% oxygen) under artificial ventilation using a rodent ventilator (Kent Scientific Co., Torrington, CT, USA). Adequacy of anesthesia was verified using a tail pinch. The heart was exposed at the fourth intercostal space, and the left anterior descending (LAD) coronary artery was occluded permanently with 7–0 polypropylene suture (Ethicon). Successful LAD occlusion was confirmed on electrocardiography (ECG) by ST-segment elevation plus cyanosis of the anterior left ventricular (LV) wall. Sham-operated mice underwent an identical surgical procedure but without LAD ligation.

2.3. Echocardiography

Echocardiograms were performed immediately before, at 24 h and 2 weeks following LAD ligation, and before sacrifice using a GE vivid7® ultrasound machine with a 12-Hz transducer (GE Healthcare, NJ, USA). Mice were anesthetized with 1.5% isoflurane, and echocardiography was performed in the parasternal short-axis view at the papillary muscle level. LV ejection fraction (EF) was used as an index of LV systolic function. All measurements were based on the average of three consecutive cardiac cycles in sinus rhythm.

2.4. Cardiac magnetic resonance imaging (MRI)

Cardiac MRI was performed at 13 weeks after sham or LAD surgeries at the UF Advanced Magnetic Resonance Imaging and Spectroscopy Facility, as described previously [17]. Briefly, following anesthesia, mice were positioned supine on a homebuilt setup that allowed monitoring of body temperature, respiratory rate, and heart rate (Small Animal Instruments). ECG electrodes were inserted into the limbs, and a respiration pad was taped across the abdomen. Mice were then maintained under anesthesia (1–1.5%) via a nose cone and were placed in the magnet. Body temperature was maintained using a regulated circulated water heater between 45 °C and 50 °C. Mice were imaged using a quadrature birdcage volume coil. A series of five transverse images were acquired over the heart after power calibration and global shimming scans. Single-slice, long-axis axial, and sagittal scans were acquired to view the heart's apex and base. These long-axis scans were used as a reference to obtain short-axis scans, which were then used to measure ventricular volumes and function. Left and right ventricles were imaged using a stack of short-axis images with 1 mm slice thickness. Images were acquired using a spoiled gradient-echo cine sequence (TR = 110 ms, TE = 1.37 ms, flip angle = 15°, field of view = 25×25 mm^2, data matrix 128×128, and 1 mm slice thickness). Twelve cine frames were acquired through the cardiac cycle in sinus rhythm and were ECG-R wave triggered.

LV function was assessed using CINE MRI images in DICOM format with Osirix medical imaging software (Pixmeo, Geneva). In total, 7–8 series of frames were acquired covering the whole heart (apex to base). End-diastolic (EDV) and end-systolic (ESV) volumes were measured for each slice and summed over the entire heart. EF was calculated as (EDV-ESV)/EDV. Composite circumferential strain (ε_{cc}%) was calculated for the base, mid, and apex level of the LV and also four apical segments as defined by the American Heart Association using the feature tracking module of segment software (Segment v2.0 2.0 R5585; http://segment.heiberg.se).

2.5. Hemodynamic measurements

High-fidelity pressure recordings were made at 4 weeks after surgery in anesthetized mice [16]. The right carotid artery was cannulated with a micromanometer catheter (Millar Instruments) advanced to the aorta then into the LV. This catheter was interfaced to a PowerLab (ADInstruments) signal transduction unit. Mean arterial pressure, LV end-diastolic pressure, maximal positive and negative rate of LV pressure rise, and heart rate were recorded using the Chart program (PowerLab system).

2.6. Micro-computed tomography (μCT) imaging the coronary vasculature

Retrograde filling of the coronary vasculature for μCT imaging was accomplished as described by others [18]. Briefly, aortic cannulation was done to assure filling of all vessels using a low viscosity radiopaque compound. This perfuses the smallest vessels to fill the capillaries and both the arterial and venous sides of the myocardial vascular network. Vessels were perfused with a buffer using a pressurized system and then filled with Microfil. To assure filling of small, higher-resistance vessels, large branches arising from the aorta were ligated to divert Microfil into the coronary arteries. Once the filling was complete, to prevent elastic recoil from squeezing Microfil out of some vessels, we ligated accessible major vascular exits immediately after filling. This optimized for complete filling and maximum retention of Microfil, enabling visualization of the entire coronary vascular network: arteries, microvasculature, and veins.

Following perfusion, animals were sacrificed, hearts explanted, and stored overnight at room temperature to ensure complete Microfil fixation. Then they were scanned with a Skyscan 1172 μCT (system/software is Bruker, Konitch, Belgium) to image the coronary vasculature. Acquisition settings were 50 kVP/200 μA, 4 K camera resolution, 3.94 μm voxel size, 0.5 mm Al filter, 0.5° rotation step, and 180° tomographic rotation. Cross-sectional images were reconstructed in NRecon using a filtered back-projection algorithm. The region of interest was defined in CTAn and encompassed the entire heart, excluding atrial and ventricular chambers. Three-dimensional region of interest images were acquired with CTVox using identical acquisition settings.

2.7. Microsphere measurements of coronary blood flow

Coronary artery blood flow and collateral perfusion were evaluated from measurements using neutron-activated microspheres (BioPal, Worcester, MA). At 1-day post LAD ligation, animals were anesthetized as noted above; the chest was reopened and 1.2×10^6 nonradioactive elementally labeled 15-μm microspheres were injected into the LV

cavity transapically. At the same time, carotid blood was simultaneously sampled at a known withdrawal rate. This dose is well below the number of spheres necessary to cause physiological effects in the heart [19]. The heart was harvested and sectioned into four radial slices from the apex to the papillary muscle, and all but the apex were quartered. This sectioning allowed analysis of blood flow, which was calculated (dpm/g) to the myocardium in the ischemic/infarcted anterior zone and the non-infarcted normally perfused zone. Tissue sections and blood samples were sent to BioPal for neutron activation [20].

2.8. Histological analysis

Under deep anesthesia and laparotomy, mice were perfused with 20 IU heparin-PBS. Hearts were collected, and the ventricles separated from the atria. Cardiac remodeling was assessed by determining ventricular hypertrophy calculated by normalizing the animal's ventricles' wet weights to their tibia length. After rinsing with $1\times$ PBS, the ventricles were weighed and cut into three different sections, perpendicular to the long axis. The basal and apex sections were snap-frozen in liquid nitrogen and stored at -80 °C for subsequent measurements. The middle section was used for histology to assess the infarct size and cardiac remodeling. Briefly, the middle section was fixed in 4% phosphate-buffered formalin, embedded in paraffin, and cut into 4 μm sections. Sections were stained with Picro-Sirius Red or Mason's Trichrome to measure fibrosis and infarct size [16]. Total infarct size was calculated as a fraction of the LV circumference.

The same reagents and identical techniques for histology and histochemistry were used on tissue sections of both species. Triphenyl tetrazolium chloride (TTC) staining was performed as above, and hearts were cut into 4 slices perpendicular to the long axis to detect and quantify the infarcted area. Each slice was rinsed briefly in 0.9% NaCl and incubated in a solution of 1% TTC in 0.2 M Tris buffer pH 7.8 for 5–7 min, photographed, then fixed.

For cell proliferative activity, 5-Bromo-2-deoxyuridine (BrdU, 50 mg/kg) was dissolved in 0.9% NaCl. Daily intraperitoneal injections were started three days post-LAD ligation and continued to 14 days. Hearts were then collected to detect BrdU incorporation, and sections were dewaxed and incubated overnight with 1.200 dilutions of a BrdU antibody (Abcam ab6326) and either used for fluorescence detection (AlexaFluor 488) or DAB detection (Vectastain Elite kit). BrdU+ cells per field were counted, and a total of six fields per animal were counted using ImageJ software. Sections were also stained with Ki67, 1 in 500 (Abcam ab16667) for proliferative activity. Other sections were double-stained with anti-sarcomeric α-actinin antibody (αSA) or PCM-1 (Abcam ab72443, 1 in 200) for cardiomyocytes (Abcam ab68167, 1 in 200) or perilipin (Abcam ab3526, 1 in 200) for adipocytes with fluorescence (AlexaFluor 488 or 647) and 4′,6-diamidino-2-phenylindole (DAPI) for nuclei.

2.9. Statistical analysis

Data were summarized and expressed as mean $\pm$ SE or percentage when appropriate and analyzed with the use of the t-test or one-way analysis of variance. Values of $p < 0.05$ were considered statistically significant. All data were analyzed using GraphPad Prism 5 software (GraphPad Prism Institute Inc).

3. Results

These experiments were based on comparisons between the adult CD1 outbred strain of *Mus musculus* as a reference and adult *Acomys cahirinus* (SM). We confirmed by visual inspection of multiple mice and μCT that the anatomy of the coronary arterial system (2-coronary arteries originating from their respective aortic sinuses) was comparable in these two distantly related rodent species.

Acomys and CD1 *Mus* also exhibited similar heart rates (CD1 433.7 $\pm$ 20.6 vs. (SM, *Acomys* 462.3 $\pm$ 12.1 BPM), systolic blood pressure (CD1 96.9 $\pm$ 7.4 vs. SM *Acomys* 103.5 $\pm$ 3.2 mmHg), and diastolic blood pressure (CD1 71.9 $\pm$ 6.9 vs. SM *Acomys* 78.8 $\pm$ 1.1 mmHg). Based on these similarities, groups of animals (each $n = 12$) from each species were subjected to LAD coronary artery ligation, and additional groups (each $n = 12$) per species served as sham-operated references that underwent identical surgical procedures but without LAD ligation.

3.1. Acomys show initial MI-induced LV dysfunction followed by recovery

Two series of experiments were performed, one in which animals were examined at one-time point (day 14) following surgery and a subsequent experiment in which the animals were examined 24-h after surgery (day 1) and then at weekly intervals to 4 weeks. Echocardiographic analyses were performed using LV EF as an index of LV systolic function.

The accumulated data (Fig. 1A) showed that immediately after LAD ligation, there was a precipitous decline in EF in both CD1 *Mus* and SM *Acomys* to 25–30% from 80 to 85%. In CD1 *Mus,* no significant improvement in EF was observed by 4 weeks, as the EF remained at 24%. In contrast, in SM *Acomys,* the EF showed significant recovery reaching 65% at 4 weeks following LAD ligation (Fig. 1A). All echocardiographic parameters are displayed in Supplement Table 1.

3.2. Collateral circulation is lost in Acomys-MI and then regenerates

Recovery of EF in the *Acomys*-MI group suggests an enhanced repair/regenerative process but could possibly result from failure to create an ischemic damaged area, perhaps due to extensive preexisting collaterals or very rapid development of collateral microvascular sprouting. However, at 24 h following LAD ligation, blood flow in areas of ischemia in the two species were very similar (Fig. 1B). Thus, collateral blood flow in ischemic-damaged regions of both species was low and comparable; therefore, differences in collateral flow were unlikely to account for EF recovery in the *Acomys*-MI group.

At 4-weeks after LAD ligation, when the EF was recovering in *SM Acomys* (Fig. 1A), retrograde filling of the coronary vasculature by μCT imaging (Fig. 1C) confirmed the expected reduction in all vessels in the distribution of the LAD in the CD1-MI vs. CD1-Sham hearts (Fig. 1C, left). In contrast, the SM *Acomys*-MI hearts appeared to have recovered a plentiful supply of smaller coronary blood vessels in the LAD distribution by 4-weeks (Fig. 1C, right).

3.3. Acomys show reduced LV remodeling after MI

Four additional groups of animals ($n = 4$ per group) were kept for longer-term analysis at 13 weeks and were assessed by MRI for cardiac function and structure. In CD1 *Mus,* the MI group had a 50% decline in EF versus sham references (CD1-MI: 32% vs. CD1-Sham: 64%) (Fig. 2A, left columns), showing a similar value to that observed at 4 weeks (CD1-MI: 28%, Fig. 1A), even though a different technique was used to measure EF. This indicates that there was no improvement in systolic function over time in CD1 mice following MI. In contrast, in SM *Acomys,* there was no significant difference in EF between reference and MI animals (SM-MI: 62% vs. SM-Sham 76%) (Fig. 2A, right columns), suggesting that the recovery of EF observed at 4 weeks (SM-MI: 68%) (Fig. 1A) effectively had been completed and there was no significant improvement in systolic function over the subsequent 9 weeks.

Next, we compared the LV wall thickness (Fig. 2B) of the infarcted areas at 13 weeks post-MI (red dotted lines in MRI images shown in Fig. 2C). The MI resulted in a 37% decrease in LV wall thickness in CD1 *Mus*-MI (CD1-MI: 0.7 mm vs. CD1 *Mus*-Sham: 1 mm) (Fig. 2B, left columns), whereas there was no significant reduction in wall thickness at this time after MI in SM *Acomys* (Fig. 2B, right columns). All MRI parameters are displayed in Supplement Table 2.
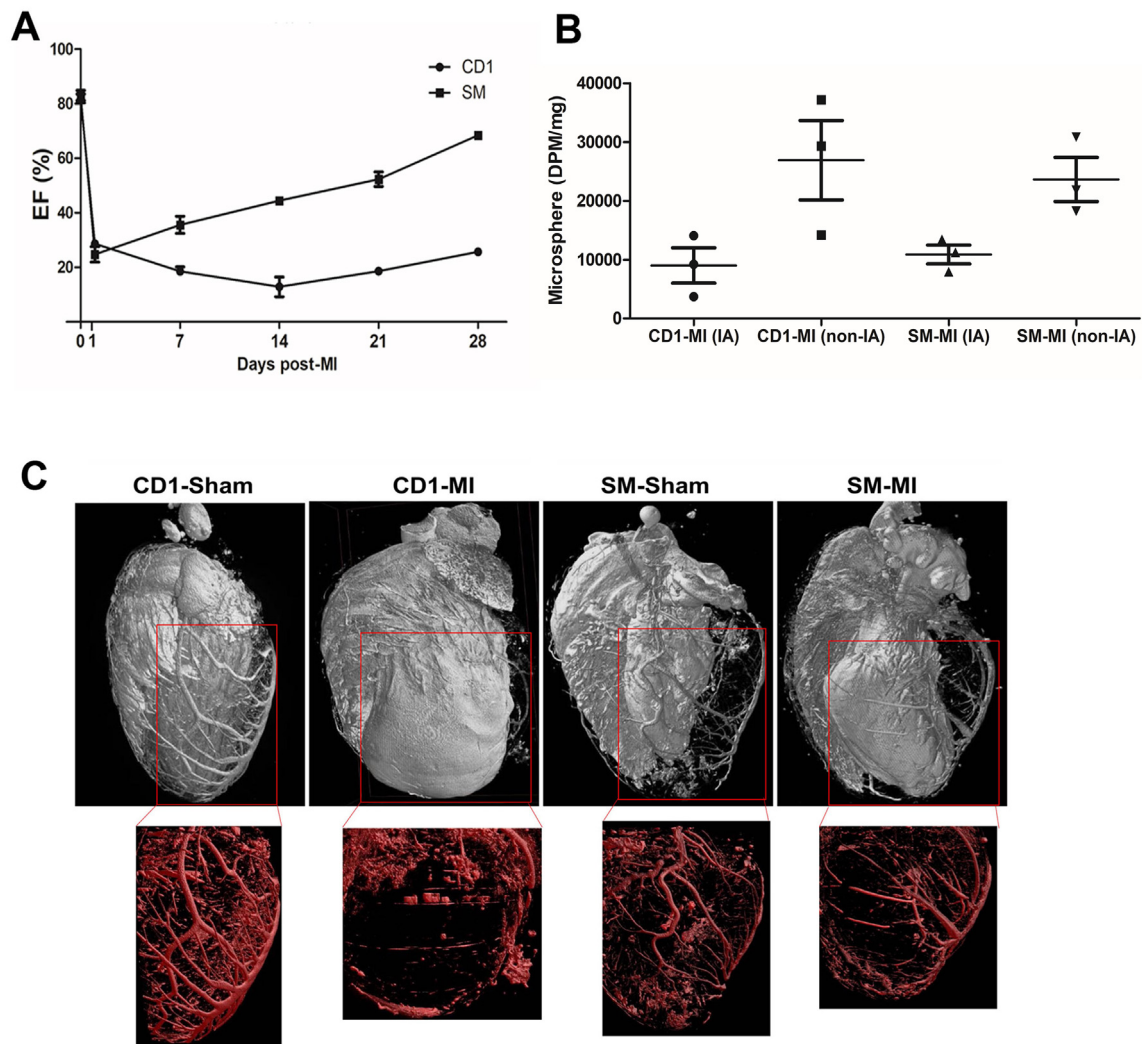
198

Fig. 1. A, echocardiographic analyses in CD1-MI (CD1) and *Acomys*-MI (SM) left ventricular ejection fraction (EF) over 4 weeks post-MI. After a similar decrease at day 1 the *Acomys* EF recovers to a value not significantly different from pre-MI values. B, quantification of the number of microsphere particles (DPM) in the ischemic areas (IA) and non-ischemic areas of the left ventricles of CD1-MI and *Acomys*-MI (SM-MI) hearts. C, representative images of μCT analyses of CD1-sham, CD1-MI, *Acomys*-sham and *Acomys*-MI hearts at 4 weeks post-MI. The SM-MI image shows that *Acomys* has regenerated the coronary vessels after MI.

We also examined the effect of infarction on regional contractile function by determining myocardial strain in the base, mid, and apical sections of the heart. In comparison to CD1 *Mus*, SM *Acomys* showed better composite ε_{cc}% production for the apex, base, and mid regions (**Supplement Fig. A**). Following MI, ε_{cc}% changed by 70% in SM *Acomys* and 88% in CD1 *Mus* within the infarcted zone (apical zone). Strain was further compared in the four apical segments from the most distal slice of the apex (**Supplement Fig. B**), and all segments of *Acomys* showed greater strain production and less worsening compared with those of CD1 *Mus* mice after MI (apical anterior- SM *Acomys* = −85%, CD1 *Mus* = −106%; apical septal- SM *Acomys* = −79%, CD1 *Mus* = −95%; apical inferior- SM *Acomys* = −55%, CD1 *Mus* = −63%; apical lateral- SM *Acomys* = −60%, CD1 *Mus* = −87%).

3.4. Histological features of LV remodeling and fibrosis

Vastly different structural features were apparent in the CD-1 *Mus* and SM *Acomys* MI hearts with Picrosirius red staining and Trichome staining (Fig. 3).

CD1 *Mus* -MI hearts showed extensive damage throughout the LV (Fig. 3A). The LV wall was thinned, containing only strands of myocardium surrounded by large areas of collagenous matrix, by trichrome staining (Fig. 3B). Interestingly, the damaged LV of these CD1 *Mus* -MI

hearts contained adipose tissue areas by perilipin staining (Fig. 3C), suggesting a defective repair response as we have observed previously in chronically damaged skeletal muscle [13].

In contrast, the damaged LV area in SM *Acomys* was considerably smaller, with most of the ventricular muscle having a thicker, more normal-appearing structure (Fig. 3D). No adipose tissue was present (Fig. 3E), and the region of remaining damage showed many small cells surrounded by cytoplasm disassociating from what appeared to be cardiac muscle fibers (Fig. 3F).

Using Picrosirius red staining, the fibrotic region of the infarction and infarct size was quantified as the percentage of the area of the free wall of the left ventricle that was fibrotic. Compared to CD-1 *Mus*, SM *Acomys* exhibited a 4-fold reduced infarct size following MI (SM *Acomys* 18% vs. CD1 *Mus* 76% LV wall infarct) (Fig. 3G) and a 3.5-fold lower ventricular wall thickness than CD1 mice (CD1 *Mus* 14.7% vs. SM *Acomys* 5.3%) (Fig. 3H).

3.5. Acomys have more proliferating cells in the LV after MI than CD1 mice

We next examined proliferative activity in various cardiac regions using both BrdU and Ki67 immunocytochemistry. BrdU counts (Fig. 4A) revealed a very low level of activity in the interventricular septum (IVS) of both CD1 *Mus* and SM *Acomys* sham hearts (boxes 1 and
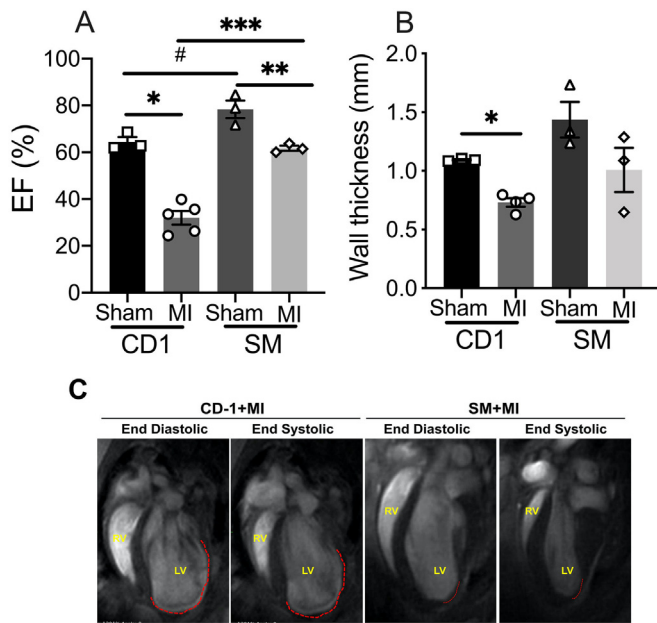
Fig. 2. A–B, bar charts with error bars showing magnetic resonance imaging (MRI) analysis in CD1 sham control, CD1 MI, SM sham (*Acomys*) control and SM MI (*Acomys*) (n = 4 per group) thirteen weeks after MI. A, left ventricular ejection fraction (EF). B, wall thickness. C, representative MRI images showing the infarct area in the left ventricle (red dotted line) in CD1 MI and *Acomys* MI groups.

2) and a small increase (2-fold over the IVS) in activity in the LV of the sham-CD1 *Mus* hearts, presumably related to damage induced when hearts were exposed through the ribs. Proliferative activity was significantly increased in the IVS of the MI hearts of both CD1 *Mus* (boxes 1 vs. 5, 6-fold increase) and the SM *Acomys* (boxes 2 vs. 6, 7-fold increase), although the absolute levels were much lower in the SM *Mus*-MI hearts. This is likely related to septal areas supplied by the LAD septal perforating branches. There was a similar level of proliferative activity in the LV free wall of the CD1 *Mus* -MI hearts vs. the IVS (boxes 5 vs. 7, 1.2-fold increase), but a very large increase in activity in SM *Acomys* MI LV free wall vs. the IVS (boxes 6 vs. 8, 8-fold increase). Comparing the free-wall of the LVs alone, there was a 2.5-fold higher level of activity in the SM *Acomys* -MI compared to the CD1 *Mus* -MI hearts (boxes 7 vs. 8). This is apparent in the representative micrograph of BrdU +ve cells in the CD1 *Mus* -MI LV, whose nuclei appeared elongated and fibroblast-like (Fig. 4C) vs. the SM *Acomys* -MI LV, whose nuclei appeared more rounded (Fig. 4D).

Proliferative activity was also obtained with Ki67 labeling (Fig. 4B). In this case, the only significant increases over proliferative activity in sham IVS and LV regions were in the CD1 *Mus* -MI IVS vs. the CD1 *Mus* -MI LV-free wall, where there was a 2-fold increase (boxes 5 vs. 7) and in the SM *Acomys* -MI IVS vs. the SM *Acomys* -MI LV-free wall, where there was a 4.5-fold increase (boxes 6 vs. 8). As with BrdU labeling, comparing the LVs alone, there was a 3.6-fold higher level of proliferative activity in the SM *Acomys* -MI vs. the CD1 *Mus* -MI hearts (boxes 7 vs. 8). Thus, similar data were obtained with BrdU and Ki67, showing that MI resulted in more widespread damage to the CD1 *Mus* heart than the SM *Acomys* MI heart, which is more localized to the LV. Also, the SM *Acomys* -MI LV had higher levels of proliferative activity vs. the CD1 *Mus* -MI LV.

The suggestion of repair seen in the SM *Acomys* LV where the cardiac muscle abuts the fibrotic region as described above (Fig. 3E, F) was also supported by double labeling with BrdU and a marker of cardiac muscle, sarcomeric α-actinin. In the SM *Acomys* -MI heart, in the area between the cardiac muscle and the fibrotic region, where there was a high level of proliferative activity occurring, double labeling showed cells that had both BrdU+ve nuclei (green in Fig. 4E) and cytoplasm +ve

for sarcomeric α-actinin (red in Fig. 4E). In this figure, 20% of the cells are double-labeled. Comparatively, in the CD1 *Mus* MI hearts, there were vanishingly small numbers of double-labeled cells, suggesting that as with the trichrome stains, there were no sites of active repair despite the increase in proliferative activity, and that perhaps those labeled cells were mostly fibroblasts. Similar data were obtained when the MI hearts were double-labeled with BrdU and another marker of cardiomyocytes, PCM1. In regions of repair in the SM *Acomys* MI tissue, double-labeled cells were seen with green nuclei (BrdU) surrounded by PCM1 (red) (white arrows in Fig. 4F, G). Other BrdU +ve/PCM1 −ve nuclei, which are seen in Fig. 4F and G, are non-cardiomyocyte cell types, likely fibroblasts and clearly in the majority.

4. Discussion

The most important and novel finding of this study is that adult spiny mice of the genus *Acomys* possess the capacity to show some restoration of cardiac function and myocardial structure following coronary artery ligation. Thus, *Acomys* is the first adult mammal with such myocardial recovery, therefore providing a unique model to investigate cardioprotective and regenerative signaling mechanisms in adult mammals.

Acomys has been previously shown to have regenerative capacity in dermal components, hair, and skeletal muscle without scarring after full-thickness skin wounds [10,11,15]. It is able to regenerate hair, skin, and cartilage after large ear punches [12,15] and does not fibrose after a skeletal muscle or kidney damage [13,14]. Because these regenerative events occur without signs of scarring, we hypothesized that *Acomys* evolved the ability *not* to induce a fibrotic response following damage. To test whether this is the case with not only skin wounds but also with damage to internal organs, we performed coronary artery ligation to induce MI in adult *Acomys*. We discovered that they could indeed recover myocardial function after this life-threatening injury.

One day after LAD ligation, both the *Mus* and *Acomys* hearts showed a large decline in LV EF, which in the *Mus* remained very low (EF = 24%) for the 13 weeks of follow-up. In contrast, the *Acomys* slowly recovered their contractile function to return to sham control EF levels by 4-weeks. Coronary microsphere studies revealed no increase in collateral circulation in *Acomys* at 24-h after LAD ligation, and μCT scans showed recovery of the coronary microvasculature in the *Acomys*-MI ventricle but not in the CD1-MI ventricle at 4 weeks. In addition to vasculature recovery, the *Acomys* LV free wall did not thin like the *Mus* ventricle, nor did the collagenous damage spread throughout the LV, resulting in a markedly reduced scar size in the SM-MI ventricle. These findings provide evidence that the *Acomys* heart can recover from substantial ischemia/infarction-related damage. This supports the concept that *Acomys* does not induce the typical fibrotic pathway that other adult mammals undergo following damage to organs and tissues. Adult *Acomys* possess a systemic *lack* of fibrotic response to wounding.

Further evidence for a regenerative response, rather than a fibrotic response, was provided by Ki67 and BrdU labeling. In both *Mus* and *Acomys*, there were increased numbers of proliferating cells in the peri-infarct region. Still, *Acomys* showed almost double the number of proliferating cells, and some were double-labeled with α-actinin, suggesting they likely were cardiomyocytes. Double labeled cells with BrdU and PCM1, another cardiomyocyte marker, also suggested that cardiomyocytes in *Acomys* can proliferate at a low level. This is similar to the response of the ventricle in both zebrafish and neonatal mouse hearts, which regenerate after physical damage or MI [3,5]. Genetic labeling studies [4,21–23] have established that the source of new cardiomyocytes in zebrafish is not a resident stem cell population, but the cardiomyocytes themselves which undergo a limited amount of dedifferentiation involving sarcomeric disorganization and expansion of intercellular spaces [3,24,25] in preparation for cell division. By 14 days after wounding, BrdU+ cell counts are 6-fold higher than in the non-regenerating heart [26]. A similar sequence of events occurs in
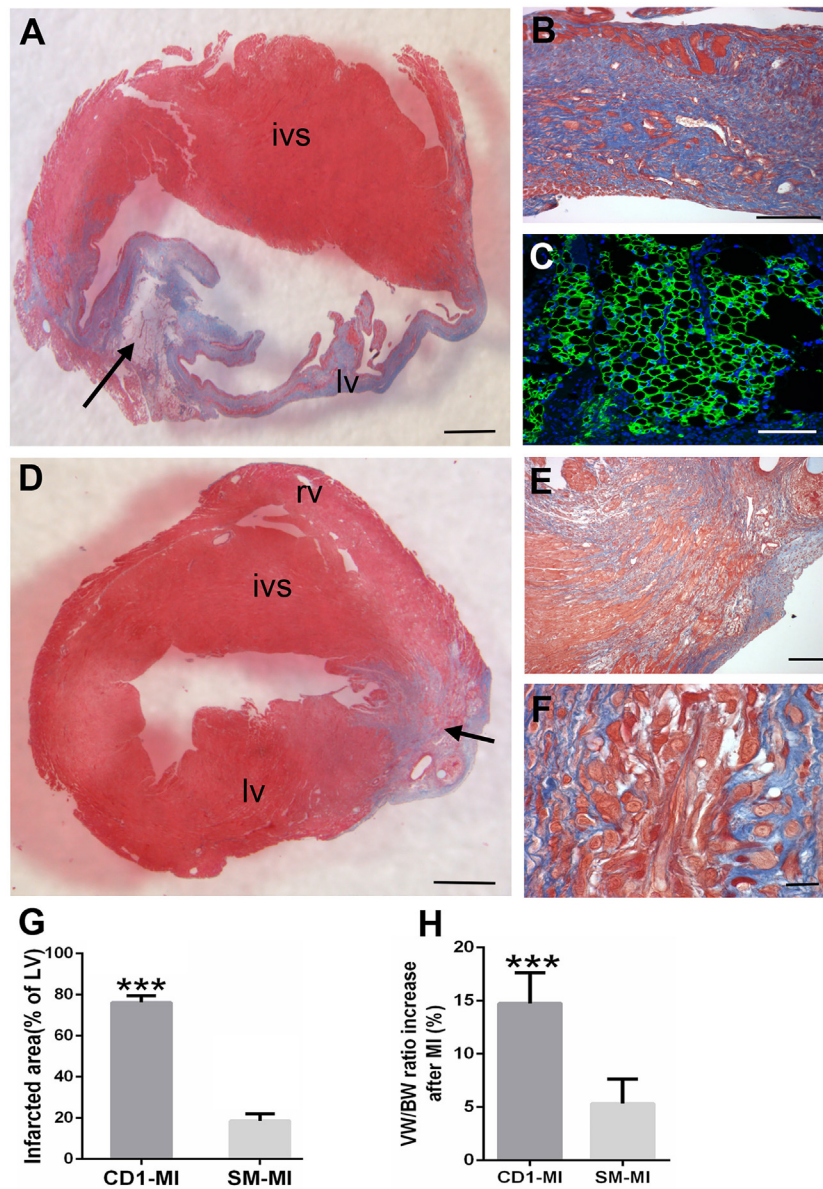
Fig. 3. A–F, representative sections through a CD1-MI heart and a SM-MI heart stained with Mason's trichrome to show areas of fibrosis (blue coloration) rv = right ventricle; ivs = interventricular septum; lv = left ventricle. A, low power section of the CD1-MI heart showing the almost complete fibrosis of the LV wall and the normal structure of the interventricular septum (IVS). Bar = 500 μm. B, high power view of the LV showing mostly blue stained collagenous matrix with small areas of surviving cardiac muscle (red). Bar = 100 μm. C, a region of adipose tissue (arrow in A) immunostained with a perilipin antibody present in the LV wall. Bar = 100 μm. D, low power section of a SM-MI heart showing only a small region of fibrosis remaining at the edge of the LV (black arrow). Bar = 500 μm. E, higher power view of the edge of the fibrotic LV region in D. F, higher power view of a region of cardiac muscle from the fibrotic region suggests that nucleated cells may be budding from muscle fibers. Bar = 20 μm. G, bar chart with error bars showing a quantification of transverse sections of CD1-MI and SM-MI (*Acomys*) hearts after Picrosirius red staining to quantify fibrotic areas as % of left ventricle. H, bar chart with error bars showing ventricular hypertrophy assessed using the ventricular weight to body weight ratio. The percentage of increase in VW/BW ratio in CD1-MI and *Acomys*-MI was calculated based on CD-Sham and *Acomys*-Sham respectively. ***$p < 0.0001$ *Acomys*-MI vs CD1-MI.

regenerating neonatal mouse heart after MI. Cardiomyocytes throughout the heart, not just at the injury site, dedifferentiate and disassemble their sarcomeres, proliferative activity is stimulated above basal levels throughout the heart (also approximately 6-fold), and the new cardiomyocytes are derived from pre-existing cardiomyocytes rather than from a resident stem cell population.

Although association has been identified in this in vivo study, a "cause-effect" strategy should be considered to further explore key components in support of the current conclusion and in vitro evidence should be collected in future studies to support the conclusion. There are many potential "cause-effect" mechanisms that could explain our preliminary data described above. To investigate these, a detailed analysis of cell type(s) responsible is firstly required. *Acomys* cardiomyocytes may fail to respond to ischemia and enter a hibernation state from

which they emerge relatively functional. *Acomys* cardiac endothelium may have different properties to rapidly respond by initiating angiogenesis to restore coronary microvasculature. Their cardiac fibroblasts may have different properties in response to ischemia and damage-induced cytokines. Molecular analyses such as RNA sequencing or single cell RNA sequencing would provide complete gene expression profiling of these differing responses which may direct our attention to particular cell types [27].

An important question centers on whether *Acomys* have better collateral flow to preserve cardiomyocytes after coronary ligation, yet we assessed collateral blood flow 1 day after MI and it was not different compared to CD-1 mice. So, it's unlikely that they have sufficiently different native collaterals to prevent cardiomyocyte death. However, we have not specifically looked at cardiomyocyte viability 1-day after MI.
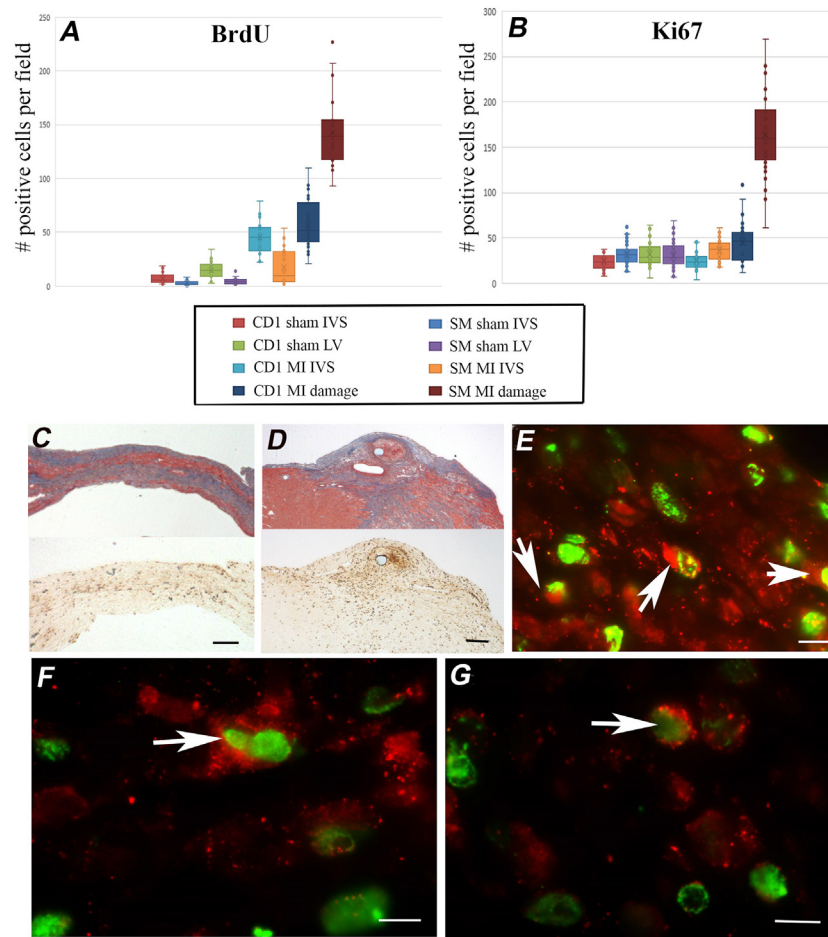
Fig. 4. A–B, Box plots of counts of labeled cells per field in various regions of the CD1 sham, CD1-MI, SM-sham (*Acomys*) and SM-MI (*Acomys*) heart using BrdU (A) or Ki67 immunocytochemistry (B). IVS = interventricular septum; L vent = left ventricle; damage = fibrotic region. Colour code of the boxes is shown below the graphs. Bars = ±SD. C, overview of the fibrotic region of a CD1-MI left ventricle (upper panel) and the BrdU stained cells in an adjacent section (lower panel) showing a significant number of +ve cells. Bar = 200 μm. D, overview of the damaged region of a SM-MI left ventricle (upper panel) and the BrdU stained cells in an adjacent section (lower panel) showing a much higher number of +ve cells than in C and that they are localized to the damaged region. Bar = 200 μm. E, the damaged region of a SM-MI left ventricle stained with BrdU (green nuclei) and sarcomeric α-actinin (red cytoplasm) showing high levels of proliferative activity (14 green nuclei) 3 of which are also have stained red in the cytoplasm (white arrows) and therefore may be proliferating cardiomyocytes. Bar = 10 μm. F–G, the damaged region of a SM-MI left ventricle stained with BrdU (green nuclei) and PCM1 (red cytoplasm) showing at least 1 nucleus in each panel which is double labeled and may therefore be a proliferating cardiomyocyte as well as several other BrdU+ve cells which are not cardiomyocytes. Bar = 10 μm.

The above studies are a key future direction for comprehensive review of potential mechanisms in the *Acomys* heart.

5. Conclusion

In summary, our analyses on adult *Acomys* ischemic/infarction damaged hearts show recovery of LV contractile function and the microvasculature, significantly reduced scarring, and increased cell proliferative activity. These findings support the suggestion of a regenerative response, or at least a decreased fibrotic response, in this adult mammal. This would be in accord with other tissues of the adult *Acomys* body, including skin, ear, and skeletal muscle, suggesting that they appear to be a novel mammalian model for identification of molecular and genetic circuits involved in cardiac protection and regeneration.

Acknowledgments

Sources of funding

Disclosures

No conflicts of interest, financial or otherwise, are declared by the authors.

Data availability statement

Most of the data underlying this article are available in the article and in its online supplementary material. Other data underlying this article will be shared on reasonable request to the corresponding author.

Appendix A. Supplementary data

Supplementary data to this article can be found online at https://doi.org/10.1016/j.ijcard.2021.06.015.

References

[1] E.J. Benjamin, P. Muntner, A. Alonso, M.S. Bittencourt, C.W. Callaway, A.P. Carson, A.M. Chamberlain, A.R. Chang, S. Cheng, S.R. Das, F.N. Delling, L. Djousse, M.S.V. Elkind, J.F. Ferguson, M. Fornage, L.C. Jordan, S.S. Khan, B.M. Kissela, K.L. Knutson, T.W. Kwan, D.T. Lackland, T.T. Lewis, J.H. Lichtman, C.T. Longenecker, M.S. Loop, P.L. Lutsey, S.S. Martin, K. Matsushita, A.E. Moran, M.E. Mussolino, M. O'Flaherty, A. Pandey, A.M. Perak, W.D. Rosamond, G.A. Roth, U.K.A. Sampson, G.M. Satou, E.B. Schroeder, S.H. Shah, N.L. Spartano, A. Stokes, D.L. Tirschwell, C.W. Tsao, M.P. Turakhia, L.B. VanWagner, J.T. Wilkins, S.S. Wong, S.S. Virani, American Heart Association Council on Epidemiology and Prevention Statistics Committee and Stroke Statistics Subcommittee, Heart Disease and Stroke Statistics-2019 Update: a report from the American Heart Association, Circulation 139 (2019), e56-e528, https://doi.org/10.1161/CIR.0000000000000659.

[2] M.J. Foglia, K.D. Poss, Building and re-building the heart by cardiomyocyte proliferation, Development 143 (2016) 729–740, https://doi.org/10.1242/dev.132910.

[3] C. Jopling, E. Sleep, M. Raya, M. Marti, A. Raya, J.C. Izpisua Belmonte, Zebrafish heart regeneration occurs by cardiomyocyte dedifferentiation and proliferation, Nature 464 (2010) 606–609, https://doi.org/10.1038/nature08899.

[4] K. Kikuchi, V. Gupta, J. Wang, J.E. Holdway, A.A. Wills, Y. Fang, K.D. Poss, tcf21+ epicardial cells adopt non-myocardial fates during zebrafish heart development and regeneration, Development 138 (2011) 2895–2902, https://doi.org/10.1242/dev.067041.

[5] E.R. Porrello, A.I. Mahmoud, E. Simpson, J.A. Hill, J.A. Richardson, E.N. Olson, H.A. Sadek, Transient regenerative potential of the neonatal mouse heart, Science 331 (2011) 1078–1080, https://doi.org/10.1126/science.1200708.

[6] J.C. Garbern, R.T. Lee, Cardiac stem cell therapy and the promise of heart regeneration, Cell Stem Cell 12 (2013) 689–698, https://doi.org/10.1016/j.stem.2013.05.008.

[7] J.H. van Berlo, J.D. Molkentin, An emerging consensus on cardiac regeneration, Nat. Med. 20 (2014) 1386–1393, https://doi.org/10.1038/nm.3764.

[8] S.E. Senyo, M.L. Steinhauser, C.L. Pizzimenti, V.K. Yang, L. Cai, M. Wang, T.D. Wu, J.L. Guerquin-Kern, C.P. Lechene, R.T. Lee, Mammalian heart renewal by pre-existing cardiomyocytes, Nature 493 (2013) 433–436, https://doi.org/10.1038/nature11682.

[9] K. Bersell, S. Arab, B. Haring, B. Kuhn, Neuregulin1/ErbB4 signaling induces cardiomyocyte proliferation and repair of heart injury, Cell 138 (2009) 257–270, https://doi.org/10.1016/j.cell.2009.04.060.

[10] J.O. Brant, M.C. Lopez, H.V. Baker, W.B. Barbazuk, M. Maden, A comparative analysis of gene expression profiles during skin regeneration in Mus and Acomys, PLoS One 10 (2015), e0142931, https://doi.org/10.1371/journal.pone.0142931.

[11] J.O. Brant, J.H. Yoon, T. Polvadore, W.B. Barbazuk, M. Maden, Cellular events during scar-free skin regeneration in the spiny mouse, Acomys, Wound Repair Regen. 24 (2016) 75–88, https://doi.org/10.1111/wrr.12385.

[12] T.R. Gawriluk, J. Simkin, K.L. Thompson, S.K. Biswas, Z. Clare-Salzler, J.M. Kimani, S.G. Kiama, J.J. Smith, V.O. Ezenwa, A.W. Seifert, Comparative analysis of ear-hole closure identifies epimorphic regeneration as a discrete trait in mammals, Nat. Commun. 7 (2016) 11164, https://doi.org/10.1038/ncomms11164.

[13] M. Maden, J.O. Brant, A. Rubiano, A.G.W. Sandoval, C. Simmons, R. Mitchell, H. Collin-Hooper, J. Jacobson, S. Omairi, K. Patel, Perfect chronic skeletal muscle regeneration in adult spiny mice, Acomys cahirinus, Sci. Rep. 8 (2018) 8920, https://doi.org/10.1038/s41598-018-27178-7.

[14] D. Okamura, C. Brewer, P. Wakenight, N. Bahrami, K. Bernardi, A. Tran, J. Olson, X. Shi, A. Piliponsky, B. Nelson, D. Beier, K. Millen, M. Majesky, Scarless repair of acute and chronic kidney injury in African Spiny mice (Acomys cahirinus), BioRxiv 315069 (2018) https://doi.org/10.1101/315069.

[15] A.W. Seifert, S.G. Kiama, M.G. Seifert, J.R. Goheen, T.M. Palmer, M. Maden, Skin shedding and tissue regeneration in African spiny mice (Acomys), Nature 489 (2012) 561–565, https://doi.org/10.1038/nature11499.

[16] Y.F. Qi, J. Zhang, L. Wang, V. Shenoy, E. Krause, S.P. Oh, C.J. Pepine, M.J. Katovich, M.K. Raizada, Angiotensin-converting enzyme 2 inhibits high-mobility group box 1 and attenuates cardiac dysfunction post-myocardial ischemia, J. Mol. Med. (Berl). 94 (2016) 37–49, https://doi.org/10.1007/s00109-015-1356-1.

[17] S. Der Sarkissian, J.L. Grobe, L. Yuan, D.R. Narielwala, G.A. Walter, M.J. Katovich, M.K. Raizada, Cardiac overexpression of angiotensin converting enzyme 2 protects the heart from ischemia-induced pathophysiology, Hypertension 51 (2008) 712–718, https://doi.org/10.1161/HYPERTENSIONAHA.107.100693.

[18] J.J. Weyers, D.D. Carlson, C.E. Murry, S.M. Schwartz, W.M. Mahoney Jr., Retrograde perfusion and filling of mouse coronary vasculature as preparation for micro computed tomography imaging, J. Vis. Exp. (2012), e3740, https://doi.org/10.3791/3740.

[19] C.P. Reinhardt, S. Dalhberg, M.A. Tries, R. Marcel, J.A. Leppo, Stable labeled microspheres to measure perfusion: validation of a neutron activation assay technique, Am. J. Physiol. Heart Circ. Physiol. 280 (2001) H108–H116, https://doi.org/10.1152/ajpheart.2001.280.1.H108.

[20] B.R. Shepherd, H.Y. Chen, C.M. Smith, G. Gruionu, S.K. Williams, J.B. Hoying, Rapid perfusion and network remodeling in a microvascular construct after implantation, Arterioscler. Thromb. Vasc. Biol. 24 (2004) 898–904, https://doi.org/10.1161/01.ATV.0000124103.86943.1e.

[21] J.M. Gonzalez-Rosa, M. Peralta, N. Mercader, Pan-epicardial lineage tracing reveals that epicardium derived cells give rise to myofibroblasts and perivascular cells during zebrafish heart regeneration, Dev. Biol. 370 (2012) 173–186, https://doi.org/10.1016/j.ydbio.2012.07.007.

[22] K. Kikuchi, J.E. Holdway, A.A. Werdich, R.M. Anderson, Y. Fang, G.F. Egnaczyk, T. Evans, C.A. Macrae, D.Y. Stainier, K.D. Poss, Primary contribution to zebrafish heart regeneration by gata4(+) cardiomyocytes, Nature 464 (2010) 601–605, https://doi.org/10.1038/nature08804.

[23] J. Wang, D. Panakova, K. Kikuchi, J.E. Holdway, M. Gemberling, J.S. Burris, S.P. Singh, A.L. Dickson, Y.F. Lin, M.K. Sabeh, A.A. Werdich, D. Yelon, C.A. Macrae, K.D. Poss, The regenerative capacity of zebrafish reverses cardiac failure caused by genetic cardiomyocyte depletion, Development 138 (2011) 3421–3430, https://doi.org/10.1242/dev.068601.

[24] F. Laube, M. Heister, C. Scholz, T. Borchardt, T. Braun, Re-programming of newt cardiomyocytes is induced by tissue regeneration, J. Cell Sci. 119 (2006) 4719–4729, https://doi.org/10.1242/jcs.03252.

[25] E.R. Porrello, A.I. Mahmoud, E. Simpson, B.A. Johnson, D. Grinsfelder, D. Canseco, P.P. Mammen, B.A. Rothermel, E.N. Olson, H.A. Sadek, Regulation of neonatal and adult mammalian heart regeneration by the miR-15 family, Proc. Natl. Acad. Sci. U. S. A. 110 (2013) 187–192, https://doi.org/10.1073/pnas.1208863110.

[26] A. Lepilina, A.N. Coon, K. Kikuchi, J.E. Holdway, R.W. Roberts, C.G. Burns, K.D. Poss, A dynamic epicardial injury response supports progenitor cell activity during zebrafish heart regeneration, Cell 127 (2006) 607–619, https://doi.org/10.1016/j.cell.2006.08.052.

[27] Y. Qi, R. Goel, A.S. Mandloi, R. Vohra, G. Walter, Y.F. Joshua, T. Gu, M.J. Katovich, J.M. Aranda, M. Maden, M.K. Raizada, C.J. Pepine, Spiny mouse is protected from ischemia-induced cardiac injury: leading role of microRNAs. Presented at Experimental Biology annual meeting, April 22–26, Chicago, FASEB J. 31 (1 Suppl) (2017) 721.4.